Int. J. Heat Mass Transfer. Vol. 36, No. 17, pp. 4233–4246, 1993
Printed in Great Britain

0017–9310/93 $6.00 + 0.00

Unsteady convective flows in a vertical slot containing variable viscosity fluids

FALIN CHEN and C. H. WU
Institute of Applied Mechanics, National Taiwan University, Taipei, Taiwan 10764, R.O.C.

(*Received* 7 *December* 1992 *and in final form* 18 *March* 1993)

Abstract—The convective flow in the vertical slot heated from one side and cooled from the other has been studied experimentally. The experiments were carried out in a tank 40 cm high × 15 cm deep × 2 cm wide containing glycerin–water solutions with concentrations ranging from 40 to 90% glycerin. It was found that unsteady convective motions prevail after the primary flow gives up its stability to multi-cellular convection. Several forms of unsteady vortex motion were identified by observing the flow patterns with a large scale schlieren system; they are, mergence of secondary vortices, collapse and degeneration of a tertiary vortex, and a sequence of vortex merging-and-unmerging leading to the turbulent flow. Such phenomena have not been reported in previous numerical or experimental investigations and are believed to be a result of varying viscosity and large Prandtl number. The critical Rayleigh numbers for transitions between different flow regimes were also determined by noting how the heat flux varied as the temperature difference across the slot was changed. In the laminar flow regime, the Nusselt number and the logarithm of Rayleigh number essentially hold a linear relationship, which is independent of Prandtl number and flow patterns.

1. INTRODUCTION

NATURAL convection in a vertical slot heated from one side and cooled from the other has been a research subject for several decades. The understanding of the convective flow and its transition is of great importance in both practical and fluid dynamical senses. In the practical sense, the present subject is crucial for the design of heat exchangers and thermal insulations because the heat transfer across the slot varies with flow structure. In the fluid dynamical sense, the affluence of flow phenomena occurring during the transition from laminar flow to turbulent flow [1, 2] provide valuable information for understanding the flow resulting from interaction between buoyancy and shearing forces, an important phenomenon existing in many geophysical and astrophysical systems.

According to the experiment of Elder [1], there are four different flow regimes occurring during the process from initially quiescent state to turbulent flow as Rayleigh number R increases. The Rayleigh number is defined as

$$R = \frac{g\alpha\Delta T H^3}{\nu\kappa}, \tag{1}$$

where g is the gravitational acceleration, α the thermal expansion coefficient, ΔT the temperature difference between two vertical walls, H the width of the slot, ν the kinematic viscosity, and κ the thermal diffusivity of the fluid. As R increases beyond zero, the fluid starts to move and results in a flow with cubic velocity profile and linear temperature distribution across the slot, which is the so-called conduction regime [3]. As R increases further, the convective motion is largely confined to the boundary layers along two vertical walls while the region between these two layers is nearly motionless and stably stratified in temperature. This is referred to as the boundary layer regime [4]. When R is increased exceeding the first critical value R_1, the central core breaks into a number of convection cells (or secondary vortices, Fig. 1(a); note that the width of the picture accounts for the width of the slot, which is 2 cm for the present study), each sloping down from the hot wall to the cold wall, consisting the secondary flow regime. For R larger than the second critical value R_2, a counter-rotating convection cell occurs between two secondary vortices, which is called the tertiary vortex and the corresponding flow called the tertiary flow (Fig. 1(b)). As R increases beyond the third critical value R_3, the tertiary flow breaks down and leads to a fully irregular turbulent flow (Fig. 1(c)).

A large number of investigations have been devoted to this subject in the past, see, for example, the extensive reviews by Lee and Korpela [5] and Le Quere [6, 7]. The unsteadiness of the convective flow in a vertical slot, however, has been paid relatively less attention but plays an important role in transition between laminar and turbulent flows. We shall thus in this study investigate unsteady convective motion in a vertical slot through an experimental approach. The unsteadiness of convection under some circumstances is in fact one of the intrinsic features of the flow in the vertical slot. It has been shown by linear stability analysis that the conduction regime is prone to an instability, which could lead to the secondary flow regime of unsteady feature. For example, for the fluid

NOMENCLATURE

a	wave number
g	gravitational acceleration constant
H	width of slot
Nu	Nusselt number
Pr	Prandtl number, ν/κ
R	Rayleigh number, equation (1)
T	temperature.

Greek symbols

α	thermal expansion coefficient
ΔT	temperature difference between vertical walls
κ	thermal diffusivity
ν	kinematic viscosity.

Subscripts

1	critical value between primary and secondary flows
2	critical value between secondary and tertiary flows
3	critical value between tertiary and turbulent flows.

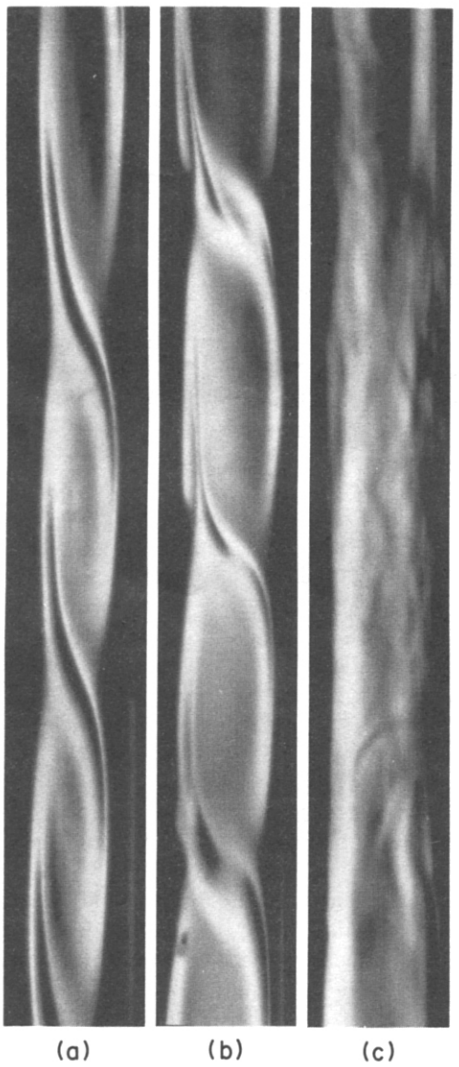

FIG. 1. Typical flow patterns for three different flow regimes: (a) secondary flow, photo taken for the 80% solution case at $\Delta T = 40.37^{\circ}$C ($R = 9.31 \times 10^5$); (b) tertiary flow, for 80% solution at $\Delta T = 66.47^{\circ}$C ($R = 15.32 \times 10^5$); (c) turbulent flow, for 50% solution at $\Delta T = 51.6^{\circ}$C ($R = 43.68 \times 10^5$).

with Prandtl number less than $Pr^c \approx 12.4$ [8], the onset of secondary flow is steady, whereas for $Pr > Pr^c$, the increasing thermal effect leads to a traveling wave instability. Nonlinear convection in a vertical slot containing large Pr fluid has been investigated analytically by Daniels [9, 10] and Daniels and Weinstein [11], in which the asymptotic structure of the flow for large R was clearly illustrated.

In addition to Pr, the appearance of unsteady secondary vortex has also been attributed to the breaking of the odd-symmetry of the base velocity and temperature profiles, which is the case if either the fluid viscosity is a function of temperature [12] or the radiative interaction is taken into account [13]. The aspect ratio of the slot was found [14] to be another factor triggering the unsteadiness of present problem. It was predicted that for a high Pr fluid ($Pr > 1000$), the flow is unstable to traveling disturbances at $R \approx 3.1 \times 10^6$ for a slot with aspect ratio 20. The unsteadiness mentioned above is mostly related to the onset of secondary flow. Although experimental works such as Elder [1], Vest and Arpaci [15], Hart [16], Seki *et al.* [17], Chen and Thangam [18], and Simpkins and Godreau [19], have been implemented in a broad range of Pr, little about the supercritical unsteadiness was reported. We thus conducted a series of experiments in the finite box of aspect ratio 20 using glycerin–water solutions to study the unsteady convective flow in vertical slot. The use of glycerin–water solution is due to the fact that its viscosity is a function of temperature, which breaks the odd-symmetry of velocity of the base flow and thus will trigger the unsteadiness of the convective motion. We employed a schlieren system to visualize the flow, from which the flow structure as well as its evolution can be clearly observed. As a result, it was found that the secondary flow occurs in a form of unsteady traveling wave motion for all the cases considered. Moreover, several unsteady vortex motions which were not reported previously, such as mergence of secondary vortices, interaction between secondary and tertiary vortices, sequence of vortex merging-and-unmerging leading to

a fully irregular turbulent flow, were uncovered by the present study. In addition, by detecting the heat flux during the progress of an experiment, we were able to determine the critical Rayleigh numbers corresponding to the transition between different flow regimes and also identified the heat transfer characteristics in terms of the relation between Nusselt number and Rayleigh number. The mechanisms driving the unsteadiness were also discussed. Present results provide new information about the unsteadiness of natural convection in the vertical slot and may help us to understand more about the fluid mechanics of the interaction between buoyancy and shear forces.

In this paper, the experimental setup is described in Section 2, a qualitative description of the evolution of flow patterns is reported in Section 3, in which an extensive discussion about the driving mechanism of unsteady flows is provided. In Section 4, quantitative results about the critical condition of transition, the heat transfer characteristics, and the hysteresis features are discussed. Finally, in Section 5 a summary of the present results is provided.

2. EXPERIMENTAL APPARATUS AND PROCEDURE

The experiments were performed in a box having inside dimensions of 40 cm high × 15 cm deep × 2 cm wide. The two vertical side walls were of sandwich construction consisting of an outer plate made of 2 cm thick plexiglas and an inner plate made of 2 cm thick brass, in which water passages were provided so that the temperature of the wall can be maintained at a constant value by separate constant temperature water baths. Under the surface of the brass plate facing the slot, sufficient material was removed to form a cavity to accommodate an ITI thermal flux sensor model B-723. The sensor being $5 \times 5 \times 0.2$ cm^3 was buried into a 0.5 cm deep cavity in which Dow Corning Silicone heatsink compound was embedded to ensure good heat transfer across the contact surfaces between the brass and the sensor. Then another 0.3 cm thick brass plate with the same cross section area of the cavity was placed tightly on the top of the sensor and the whole wall surface facing the slot was coated with nickel. The coating was also made for the other brass wall. The other two side walls facing the depth of the slot and the top and bottom walls of the slot were all made of 2 cm thick plexiglas.

Five thermalcouples were used to monitor the temperature of each brass wall, on which the measured temperatures located near the top and the bottom of the slot used differed by less than 1°C. The heat flux output as well as the thermalcouple signals were received and analyzed by a computer front end Fluke 2289 and a personal computer, in which the resultant data were recorded. The heat flux sensor was calibrated in the same box by lying the box horizontally and heating from above and cooling from below. Water was used as the working fluid as calibration was performed. Two Lauda constant temperature circulators were employed to maintain the wall temperatures to be constant. For the cold wall, a larger circulator Model RK20 was used while the hot wall was connected to a smaller circulator Model RM6. The larger circulator supplying 8 liters per min (l m^{-1}) compared with 1.6 l m^{-1} of the smaller circulator was needed for the cold wall because it was more difficult to lower the temperature than to heat it up.

A schlieren system consisting of a 100-watt Quartz Tungsten Halogen lamp, two 20 cm diameter optical lens, and an adjustable knife edge was used to observe the flow pattern in the mid-height of slot covering approximately 16 cm in height. The image of the shadow of the flow was collected on a screen which was scaled up to a suitable dimension for accommodating the image from the slot. The schlieren system was set up on a Newport optical table. The test box was insulated with black foamed rubbers on all the sides except for two slits which were left to allow the light to pass through the slot. The test solutions, glycerin–water solutions with concentration ranging from 40 to 90% glycerin, were prepared with a magnetic stirrer. After carefully pouring the solution into the box, we removed the air bubbles generated during the pouring as well as the stirring and waited until the fluid motion vanished before starting the experiment. We started with a uniform temperature (i.e. the mean temperature T_0, see Table 1) and increased the hot wall temperature and decreased the cold wall temperature by the same amount before the cold wall temperature reached about 6°C, after which the cold wall temperature was maintained constant while the hot wall temperature was adjusted to a desirable ΔT. The hot wall temperature had never exceeded 90°C.

For each different solution, three to six experimental runs were performed. Adjustments in ΔT were made every hour, according to the thermal diffusion time of the solution. Each ΔT was determined by the averaged value of the five thermcouple readings on

Table 1. Physical properties of glycerin–water solutions used in the present study

	90%	80%	70%	60%	50%	40%
T_0(°C)	40	35	30	25	25	25
$\kappa \times 10^6$ (m^2 s^{-1})	0.0854	0.0903	0.0964	0.1014	0.1054	0.1114
$\nu \times 10^6$ (m^2 s^{-1})	49.07	22.81	12.18	7.666	4.486	2.900
$\alpha \times 10^3$ (°C^{-1})	0.630	0.605	0.560	0.550	0.510	0.445
Pr	574.6	252.6	126.4	75.60	42.56	26.03

each wall and the averaged values were recorded on the hard disc every ten seconds for two minutes. Then the temporal–spatial-averaged wall temperatures were used to determine the ΔT. Similarly, the heat flux value was also determined by the same time average procedure. We also measure the wavelength of the convection cell on the screen. Since, as will be discussed later, the convective motion used to appear unsteadily, the measurement of wavelength was always accompanied with a relatively large uncertainty. The evolution of flow patterns as ΔT changes were carefully observed as well as photoed by a Nikon F4 camera.

3. OBSERVATIONS OF FLOW PATTERN FORMATION

Theoretically, a convective flow is generated as soon as the ΔT is greater than zero. From the schlieren system, however, either the large circulation of the convective flow in the conduction regime or the boundary layer flow in the boundary layer regime was not observable, although it was seen that the shadows near the two vertical walls became increasingly thicker as the flow switched from the conduction regime to the boundary layer regime. As the secondary vortex occurred, the shadows collected by the schlieren system reflecting the first order gradient of fluid density variation became discernible. For all the cases considered, the onset of secondary vortex appeared to be unsteady. The convection cells used to be first observed near the mid-height of the slot and drifted upwards slowly. Similar unsteady convection also occurred in the tertiary flow regime. In the following of this section, we report several unsteady vortex motions which play a significant role in describing the unsteady convection within the vertical slot. Each picture shown was taken from the central part of the slot. The width of each picture accounts for the width of the slot, i.e. 2 cm, and the height covers more than 15 cm crossing the mid-height of the slot.

3.1. *Typical flow patterns at different Rayleigh numbers*

Although the convection was unsteady, we were still able to identify the typical flow patterns at different R. Figure 2 illustrates a series of flow patterns corresponding to different R for a 90% solution. Each picture was taken as convection cells shown on the screen appeared to be approximately uniform in size. Since the traveling wave speed of convection cells was much slower than the convective flow velocity, the flow patterns as shown in the figure could be sustained for quite a while. Figures 2(a)–(c) show the secondary vortices whose wavelengths were generally increasing with R. In Figs. 2(d)–(f), tertiary cells occurred and increased in size as R increased.

To gain physical insights into the occurrence of secondary and tertiary vortices, we consider the boundary-layer regime in a finite cavity. Since boundary layers form on the vertical walls and compete for fluid, the layer on the warmer wall entrains fluid from the lower half of the slot while the layer on the cooler wall entrains fluid from the upper half. The entrainment induces a horizontal cross flow in the core region and leads to a vertical temperature gradient in the core. This vertical gradient profoundly influences the structure of boundary layers on the wall. As the boundary layer structure changes, the pitch of the flow entrainment reduces so that the core flow changes from a large circulation into several small circulations, i.e. the secondary vortices. As R increases, the circulation of secondary vortex increases. Since these vortices circulate in the same direction, there is a strong shear force acting on the interface between vortices, which turns out to be quite unstable. As a result, a counter-rotating tertiary vortex occurs between secondary vortices to release the stress gradient across the interface.

3.2. *Mergence of secondary cells*

Since secondary cells circulated in the same direction, usually sloping down from the hot wall to the cold wall, the interface between two cells was rather unstable due to the vigorous shear force. As the interface surface became unstable, the convective flows in two cells impinged on each other at the interface and eventually the circulation near the interface vanished. As a result, two secondary vortices merged together and a larger cell was formed. Figures 3(a)–(f) illustrate the evolution of the mergence, which took about 2 min (Figs. 3(a)–(e)) to complete the merging process and another 11 min for the cells to return to the original wavelength (Fig. 3(f)).

3.3. *Collapse of a tertiary cell*

As the secondary vortex became increasingly stronger as R increased, the instability of the interface between secondary cells resulted in a counter-rotating tertiary cell, which served to extinguish the strong shear force at the interface and thus inhibited the instability of interface. Nevertheless, the tertiary cell itself turned out to be rather unstable. The instability of the tertiary cell led to several different kinds of unsteadiness of the convective flow, which are described in the following.

3.3.1. *Disappearance leading to mergence of secondary cells.* The first kind of unsteadiness of the tertiary cell is its disappearance, which in turn leads to a mergence of two secondary cells. Figure 4 shows the sequence of the disappearance as well as the mergence for the 80% solution at $R = 15.7 \times 10^5$. In Fig. 4(a), two tertiary cells were sitting between secondary cells while the upper one looked a little smaller. About 10 min later, the upper tertiary cell disappeared. The new interface between secondary cells never stayed stable and, eventually, collapsed in a relatively shorter time (about 2.5 min from Figs. 4(b)–(e)).

3.3.2. *Degeneration into a secondary and two tertiary cells.* Once the tertiary cell stably circulated between secondary cells, it continuously gained momentum from its neighboring cells and increased in size. As the

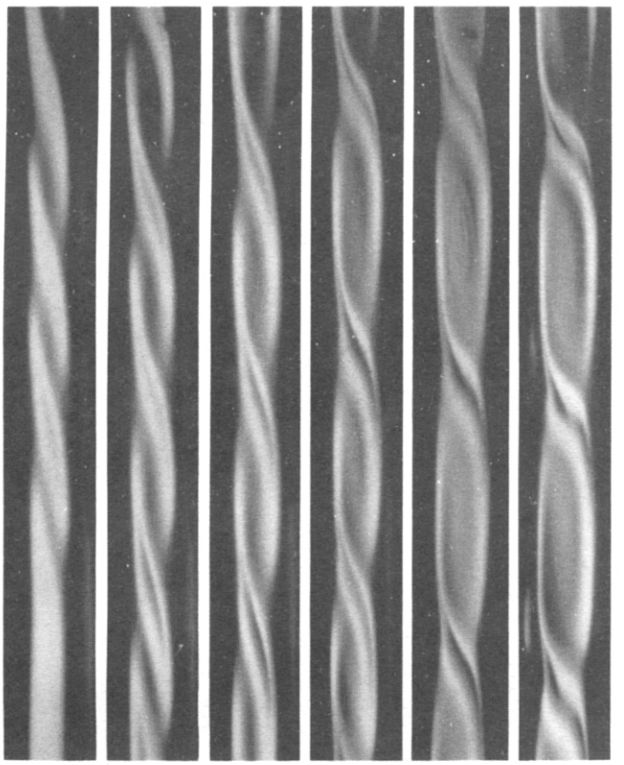

FIG. 2. Typical flow patterns at different ΔT for the 90% solution case. (a) $\Delta T = 46.69°C$ ($R = 5.51 \times 10^5$); (b) $\Delta T = 54.12°C$ ($R = 6.39 \times 10^5$); (c) $\Delta T = 61.57°C$ ($R = 7.26 \times 10^5$); (d) $\Delta T = 68.82°C$ ($R = 8.12 \times 10^5$); (e) $\Delta T = 76.04°C$ ($R = 8.97 \times 10^5$); (f) $\Delta T = 83.16°C$ ($R = 9.81 \times 10^5$).

size was approximately equal to that of the secondary cell, the tertiary cell degenerated into a secondary cell and two smaller tertiary cells. The degeneration is obviously due to the boundary condition on the vertical walls. The tertiary cell brought fluids upwards along the cold wall and downwards along the hot wall. A strong shear force gradient thus occurred across the interface between the tertiary cell and boundary layer. Accordingly, a large tertiary cell is intrinsically unstable.

Figure 5 illustrates the case of 70% solution at $R = 23.98 \times 10^5$ in which the degeneration of a tertiary cell occurred. The tertiary cell was first stretched in the vertical direction due to its instability (Figs. 5(a) and (b)). About 1.5 min later, the tertiary cell obviously tore (Fig. 5(c)) and in a short time (about 30 s later, Fig. 5(d)) a secondary cell and two tertiary cells were formed. It took another 2 min or so to stabilize the new cells (Fig. 5(e)).

3.3.3. *Combination of disappearance and degeneration.* The unsteady motions described in Sections 3.3.1 and 3.3.2 may occur in the same period if conditions are relevant. Figure 6 illustrates this possibility for a 60% solution at $R = 19.65 \times 10^5$. In Fig. 6(a), the tertiary cell at the center virtually vanished. In about 4 min (Figs. 6(b)–(d)), the two secondary cells already merged together. Meanwhile, the lower tertiary cell was stretched and, eventually, degenerated into a secondary cell and a tertiary cell (Figs. 6(e) and (f)). Note that the interface near the mid-height of the picture was unstable and would collapse about 10 min later. Consequently, the two secondary cells merged and the two tertiary cells moved closer to the center.

3.4. *Sequence of vortex merging-and-unmerging leading turbulence*

In a highly supercritical stage, the vortices in the slot are so unstable that a continuous vortex degeneration may occur and lead eventually to a fully irregular turbulent flow. A series of pictures describing such a sequence of vortex degeneration is provided in Figs. 7(a)–(m) in which a 70% solution was used and $R = 18.25 \times 10^5$. In Fig. 7(a), the convection cells were stably lying in the slot with a smaller $R = 15.72 \times 10^5$. Then the Rayleigh number (or ΔT) was adjusted to 18.25×10^5 and after waiting about 17 min (Fig. 7(b)) we observed a sequence of vortex merging-and-unmerging. In this series of pictures, the two tertiary cells (Fig. 7(b)) played a significant role in triggering the vortex degeneration. It was found that both ter-

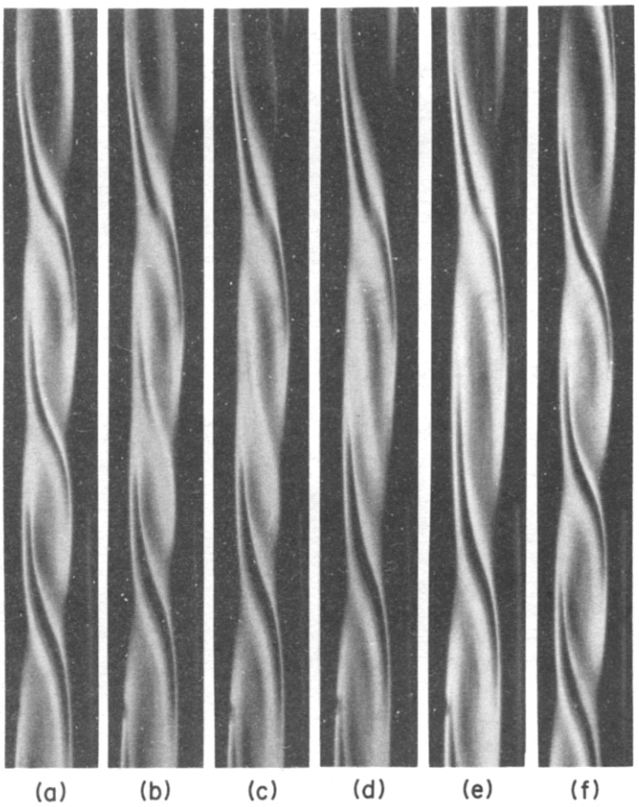

FIG. 3. The mergence of two secondary vortices for the 80% solution case at $\Delta T = 40.37^{\circ}C$ ($R = 9.31 \times 10^5$). (a) $t = 21:32:21$; (b) $t = 21:33:20$; (c) $t = 21:33:35$; (d) $t = 21:33:51$; (e) $t = 21:34:21$; (f) $t = 21:45:20$.

tiary cells were stretched simultaneously while the center one degenerated into a secondary and two tertiary cells and the upper one gradually disappeared (Figs. 7(b)–(g)). The disappearance of the upper tertiary cell induced the disruption of the secondary cell next to it (Fig. 7(h)) and in turn triggered the instability of the neighboring tertiary cell. It is of interest to note that the vortex degeneration leading to a turbulent flow is not quite a monotonic process. The pictures shown respectively in Figs. 7(h)–(j) for the center tertiary cell and in Figs. 7(k), (l) for the upper tertiary cell illustrate that the degenerated cell somehow picked up momentum from vertical boundaries and formed another cell. But, after all, the new cells were so weak in circulation that they did not sustain for too long before they collapsed. The disruption of the regularly spaced convection cells (for example, Fig. 7(m)) consequently resulted in a fully turbulent flow as shown in Fig. 1(c).

3.5. *Discussion*

We noted during the experiment that the unsteady flows described above were essentially two dimensional; namely, the variation of the flow in the deep direction is virtually negligible. These two dimensional flows are unsteady in nature, which shall be discussed later. Particularly, the onset of secondary vortex is of traveling wave type; as R increase further, the unsteadiness sustains for subsequent flows and leads eventually to a turbulent flow. Three factors, the Prandtl number, aspect ratio, and variable viscosity, are suspected to be responsible for triggering the unsteadiness of present flows; they are discussed in the following.

3.5.1. *Prandtl number effect.* Linear stability analysis predicts that for $Pr > Pr^c = 12.4$, the onset of secondary vortex motion is unsteady. To explain this in a physical sense, Hart [16], by calculating the energy integrals, showed that as Pr increases the disturbance due to buoyancy effect becomes increasingly larger than that due to the viscous effect, and results in the onset of traveling secondary cells. In the present experiment, we used fluids of $Pr > 25.6$ and thus expected the occurrence of unsteady secondary vortices, which has been confirmed by present experiments. In fact, the unsteadiness is not only possessed by the secondary vortex, but also is an intrinsic feature for subsequent flows with larger R. The subsequent flows inherited the unsteadiness of its preceding secondary flow and continuously gained the momentum for the

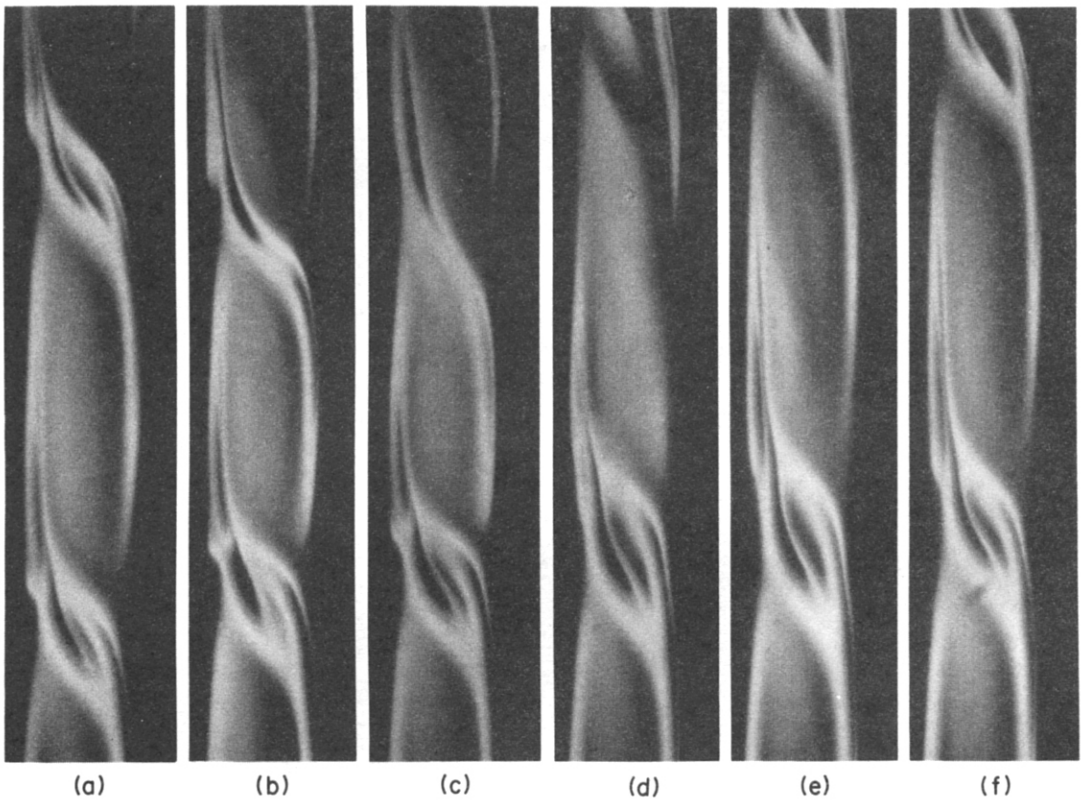

FIG. 4. The mergence of two secondary vortices with a tertiary vortex in between for the 80% solution case at $\Delta T = 68.15°C$ ($R = 15.71 \times 10^5$). (a) $t = 9:19:40$; (b) $t = 9:29:43$; (c) $t = 9:30:58$; (d) $t = 9:31:40$; (e) $t = 9:32:11$; (f) $t = 9:34:44$.

unsteady motion through the physical mechanism proposed by Hart as mentioned above.

It was found that the unsteadiness in terms of the period of merging process is dependent on Pr, R and flow patterns. Figure 8 illustrates typical examples of the period of mergence of two secondary vortices in two different situations: one with a tertiary vortex and the other without tertiary vortex. For the case of 90% solution, for instance, the tertiary vortex occurs at $R_2 \approx 7.41 \times 10^5$. For $R < R_2$, the time period (Fig. 8(a)) is approximately 4.8 min for the case without tertiary vortex. For $R > R_2$, as a tertiary vortex occurs between secondary vortices, the time period increases dramatically to about 9.5 min. This dramatic increase of the time period of merging was not observed for the case of 60% solution (Fig. 8(b)), for which $R_2 \approx 13.3 \times 10^5$. As shown in Fig. 8(b), the time period increases continuously with R because the tertiary cell is of relatively weak circulation. As a result, the existence of a tertiary cell does not significantly influence the period of mergence of secondary vortices.

3.5.2. *Aspect ratio effect.* Gill and Kirkham [14] showed theoretically that for a two dimensional vertical slot with an infinite aspect ratio, the base flow of $Pr = O(1000)$ is prone to a traveling wave instability as

$$R \geqslant 9400 Pr^{1/2}. \tag{2}$$

Present results showed (Table 2) that the first critical Rayleigh number R_1 approaches to equation (2) as $Pr \to 1000$. This implies that the aspect ratio ($=20$) of the present configuration does not cause any significant effect on the stability characteristics of the flow. The end effect is thus not a factor causing the onset of unsteady secondary vortex and thus is not believed to be influential on the unsteadiness of subsequent flows.

3.5.3. *Variable viscosity effect.* Variable viscosity breaks the odd-symmetry of the base velocity profile and causes the cells to travel upwards, because the smaller viscosity in the portion close to the hot wall results in a larger upward velocity than the downward velocity near the cold wall. The traveling cells result in an unsteady temperature distribution, which in turn induces the viscosity to change with time and space. Accordingly, that the unsteadiness is a result of interaction between buoyancy and shear forces [16] may lead us to believe that the variable viscosity effect would therefore be an important factor causing the unsteady motions observed.

Although the above implication is not evidently supported by present experimental findings, it is

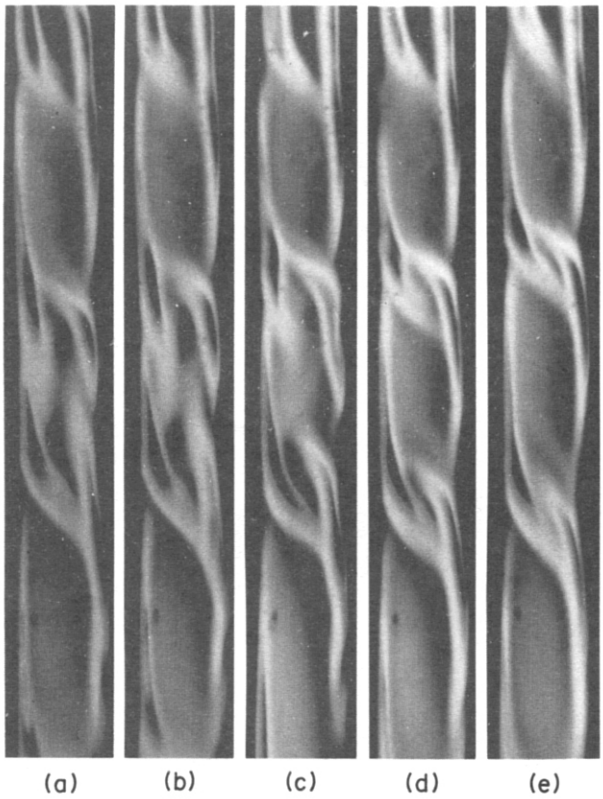

FIG. 5. The degeneration of a tertiary vortex into a secondary vortex and two tertiary vortices for the 70% solution case at $\Delta T = 64.08°C$ ($R = 23.98 \times 10^5$). (a) $t = 21:28:19$; (b) $t = 21:30:19$; (c) $t = 21:31:46$; (d) $t = 21:32:24$; (e) $t = 21:34:19$.

nevertheless believed that variable viscosity not only causes the onset of traveling secondary vortex motion, but also that it is the main mechanism driving the unsteadiness of subsequent flows. The reasons are addressed in the following. First, in previous studies for large Pr fluids [9, 10, 17, 19], no similar vortex motion as observed in the present experiment was reported because the variable viscosity effect was not considered. Secondly, for low Pr fluids, the two dimensional secondary flow gives up its stability to three dimensional oscillatory motion [20, 21]. This, however, is not the case for the present experiment since from the observation the unsteady flows were found essentially to be two dimensional in all the cases considered. Thirdly, the variable viscosity not only breaks the odd-symmetry of the base flow, but also influences the velocity profile of subsequent flows, because, in essence, the velocity depends largely on viscosity distribution, which turns out to be unsteady and asymmetric. As discussed before, the break of odd-symmetry of basic velocity profile causes the drift of secondary cells. Similarly, the unsteadiness of tertiary flow is also caused by the variable viscosity.

In summary, both the Prandtl number and variable viscosity are the main factors causing the unsteady vortex motions observed. The unsteadiness becomes more prevailing as R increases and the characteristics of unsteady motion in terms of period of mergence is dependent on R, Pr and flow patterns.

4. QUANTITATIVE MEASUREMENTS

4.1. *Critical Rayleigh numbers of transition*

We determined the critical Rayleigh numbers of the transitions from primary flow to secondary flow R_1, secondary flow to tertiary flow R_2, and tertiary flow to turbulent flow R_3 by the variation of heat flux q vs ΔT as well as by observing the flow from schlieren system. Figure 9 illustrates a typical example of q vs ΔT for a 70% solution case. In this case, the values of critical ΔT are $\Delta T_1 \approx 6°C$, $\Delta T_2 \approx 32°C$, and $\Delta T_3 \approx 61.5°C$, whose corresponding Rayleigh numbers based on the properties at the mean temperature (see Table 1) are respectively $R_1 \approx 2.25 \times 10^5$, $R_2 \approx 11.98 \times 10^5$, and $R_3 \approx 23.02 \times 10^5$. It is found that the relation between q and ΔT is linear in laminar flow regime while it is nonlinear for the turbulent flow. In the vicinities of the critical points, the change of the slope of the curve is a gradual process and therefore the curve therein is not a straight line. This is due

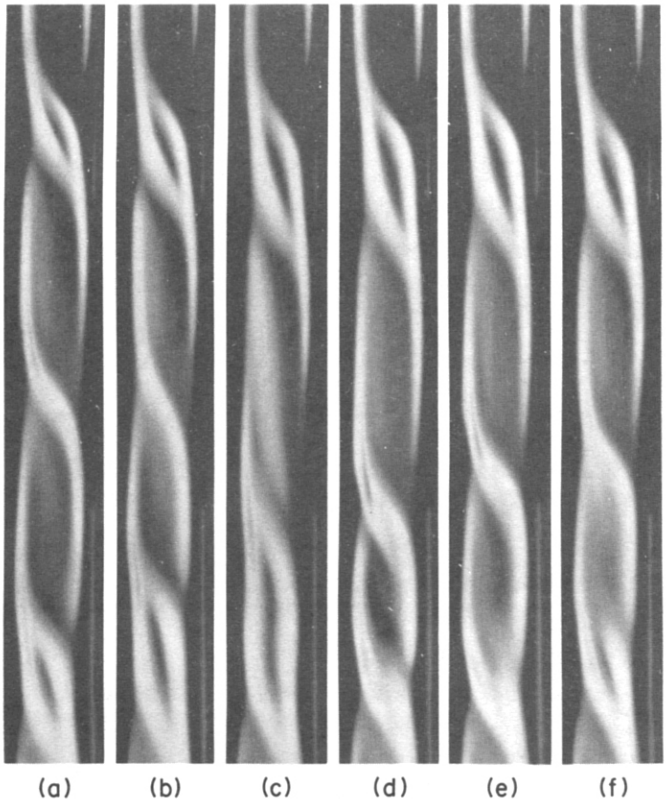

FIG. 6. The mergence of two secondary vortices and the degeneration of a tertiary vortex into a secondary vortex for the 60% solution case at $\Delta T = 35.38°C$ ($R = 19.65 \times 10^5$). (a) $t = 17:42:02$; (b) $t = 17:44:08$; (c) $t = 17:44:59$; (d) $t = 17:46:05$; (e) $t = 17:47:03$; (f) $t = 17:49:06$.

to the fact that the transitions between different flow regimes are imperfect bifurcations [9]. Note that the determinations of ΔT_1 ($\approx 6°C$) for the present case and for the cases with smaller concentration solutions were implemented in figures with enlarged scale in the small ΔT domain. The estimated error of critical ΔT is approximately within $\pm 0.1°C$.

A comparison of R_1 of present and previous studies is shown in Table 2. The R_1 of Chen and Thangam [18] were determined by the experimental observation using a shadowgraph technique and the theoretical R_1 of Chen and Pearlstein [22] were calculated by using their four-parameter fit viscosity–temperature model setup for glycerin–water solutions, in which the mean temperatures T_0 of Chen and Tangam were used. Both experimental results of Chen and Thangam and present study show that R_1 decreases with Pr (see also Seki *et al.* [17]) although the R_1 of the present study are invariably larger than those of Chen and Thangam. We note that the larger R_1 of present study is due to the higher mean temperature T_0 considered since the viscosity of glycerin–water solution decreases as temperature increases. In contrast to the experimental results, the theoretical data of Chen and Pearlstein show that R_1 increases with Pr. This discrepancy between theoretical and experimental results may be due to the fact that the theoretical analysis was implemented in an infinite vertical slot and considered a conduction basic state whereas the experiments were carried out in a finite cavity and the basic state is the boundary layer flow regime.

We summarize in Fig. 10 the values of R_1, R_2, and R_3 for all the cases considered in the present study. The error for each case was determined mainly by the uncertainty of critical ΔT. The larger error for smaller concentration solution is a result of the smaller values of ν and κ. The R_1 for the cases using 50% and 40% solutions are not available based on the resolution of the instruments of present experimental set up. Similarly, the determinations of R_3 for the cases using 80 and 90% solutions cannot be carried out since the highest hot wall temperature was usually smaller than 90°C and the lowest cold wall temperature should be greater than 6°C due to the inclusion of water in the solution.

4.2. *Heat transfer characteristics*

We convert the data of q and ΔT as shown in Fig. 9 into Nusselt number Nu and Rayleigh number R, respectively, and collect in Fig. 11 all the data of

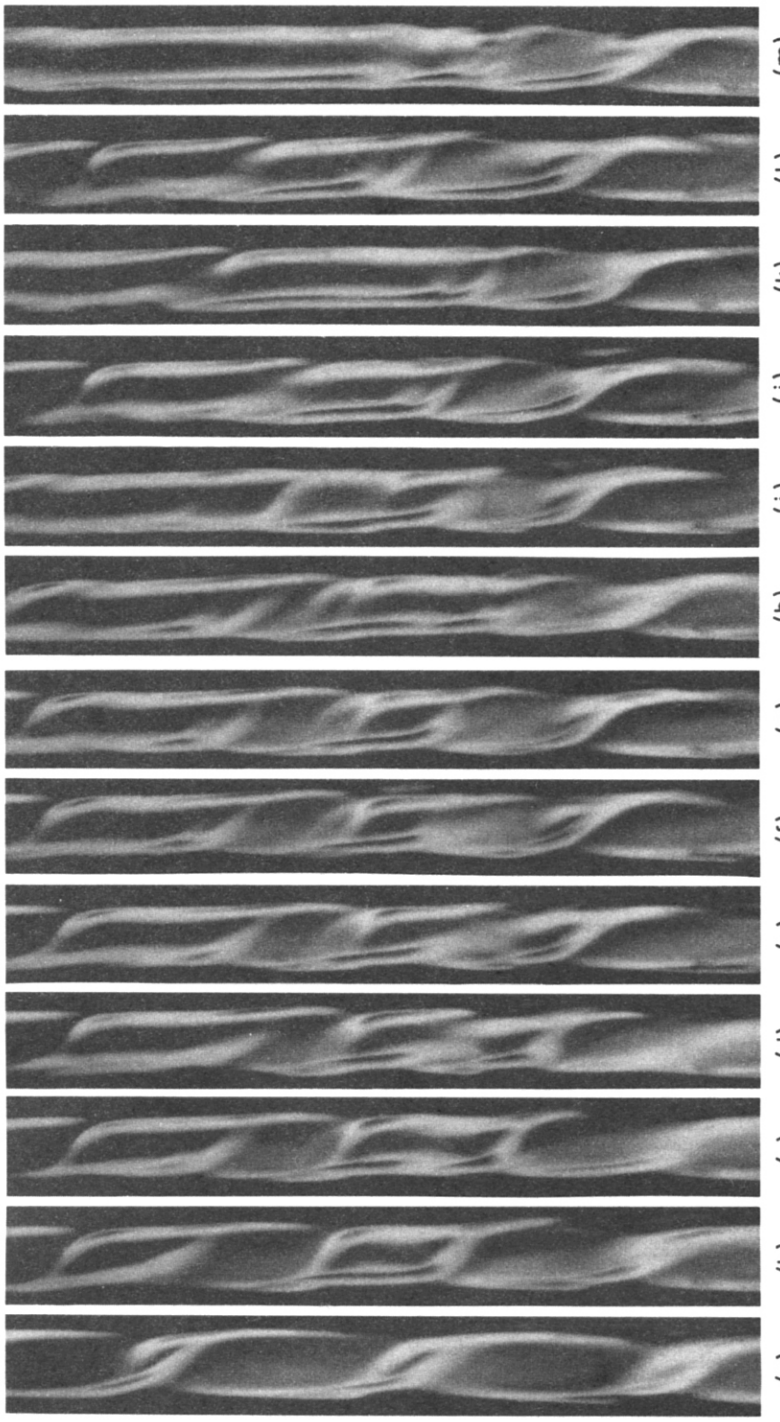

FIG. 7. A sequence of vortex breakdown leading to a turbulent flow for the 70% solution case at $\Delta T = 68.75°C$ ($R = 25.74 \times 10^5$). (a) $t = 19:20:46$ ($\Delta T = 42°C$, $R = 15.72 \times 10^5$); (b) $t = 19:37:23$; (c) $t = 19:38:53$; (d) $t = 19:39:37$; (e) $t = 19:40:23$; (f) $t = 19:40:53$; (g) $t = 19:41:23$; (h) $t = 19:43:23$; (i) $t = 19:45:22$; (j) $t = 19:51:22$; (k) $t = 19:56:37$; (l) $t = 20:05:23$; (m) $t = 20:15:58$.

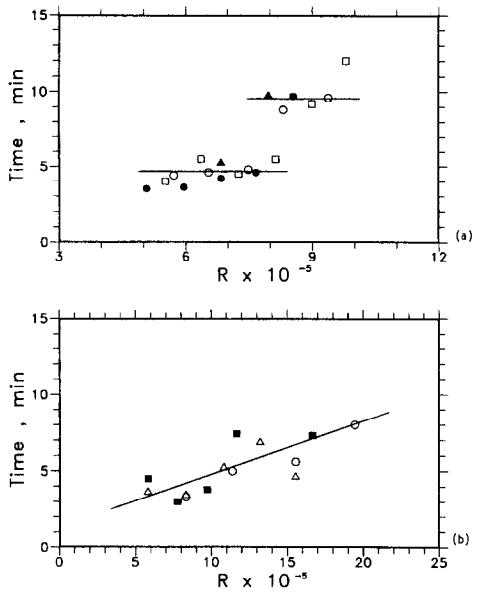

FIG. 8. Time period for the mergence of secondary vortices. (a) 90% solution; (b) 60% solution.

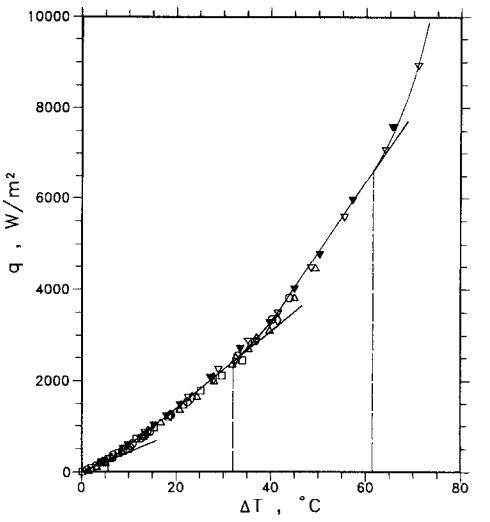

FIG. 9. The variation of heat flux q vs ΔT for the 70% solution case. The hollow markers account for the data in increasing ΔT process and the corresponding solid markers for the decreasing ΔT process of the same test.

every case considered. Note that both Nu and R were calculated based on the physical properties at corresponding mean temperature of each case (Table 1). It is seen from Fig. 11 that the relation between Nu and log (R) in laminar flow regime is linear

$$Nu = 1.89 \log R - 7.28 \quad (3)$$

which in general causes an error within 6%. The relation of equation (3) holds for different laminar flow patterns and is independent of Prandtl number. This is consistent with the experimental results of Seki *et al.* [17] for high Pr solutions and the numerical results by Le Quere [6] who considered the unsteady convection of air in a finite vertical slot with aspect ratio 16. In comparison with the current results in Fig. 11 and those of Le Quere (in his Fig. 10, note that his R scale needs to be converted into a logarithmic scale when comparison is made), it is found that the relationships of Nu with R of these two studies are quite similar except that the present heat transfer rate is generally larger than that of Le Quere [6].

Table 2. Comparison of the results of present study (A) and those of Chen and Thangam [18] (B) and Chen and Pearlstein [22] (C)

		T_0 (°C)	ΔT_1 (°C)	$R_1 \times 10^{-5}$
A	70%	30	6	2.25
	80%	35	8	1.84
	90%	40	14	1.65
B	70%	21.5	17.4	4.10
	80%	22.7	31.9	3.42
	90%	33.4	49.1	3.32
C	70%	21.5	4.0	0.94
	80%	22.7	13.8	1.48
	90%	33.4	28.7	1.94

We note that although the heat flux was measured in the mid-height of the slot (cf. the heat flux sensor is of 5 × 5 cm^2 in area) and the heat transfer rate across the slot varies vertically [5], the present heat flux measurement to some extent can still account for the heat transfer characteristics of the present configuration. Because the vertical variation of heat flux is generally quite mild except near the end of slot, which, as discussed in Section 3.5.2, has no significant effect on the hydrodynamics characteristics and is not believed to be influential on the heat transfer either. In addition, the 25 cm^2 extent should be able to cover enough area to collect representative heat transfer data. It is also noted that the validity of equation (3) holds in the region $R_1 < R < R_3$, which in Fig. 11 is

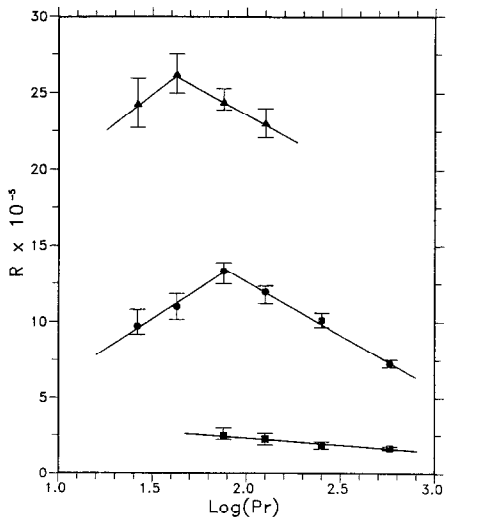

FIG. 10. The critical Rayleigh numbers for the transitions. ■: R_1; ●: R_2; △: R_3.

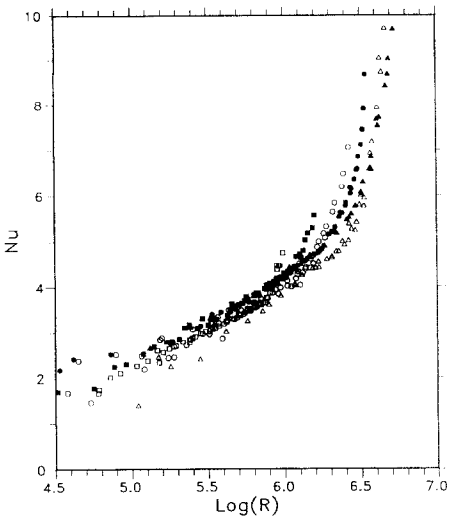

FIG. 11. The Nusselt number vs Rayleigh number for all the cases considered in the present study. □: 90% solution; ■: 80% solution; ○: 70% solution; ●: 60% solution; △: 50% solution; ▲: 40% solution.

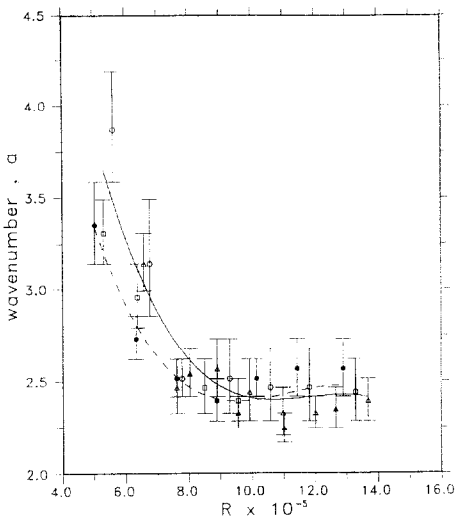

FIG. 12. The variation of wave number a vs R. — : curve fitting for the data in the increasing ΔT process; - - - : curve fitting for the data in the decreasing ΔT process.

approximately equivalent to $5.2 < \log(R) < 6.2$ (see also Fig. 10).

4.3. *Hysteresis of convection*

For low Pr fluids, both numerical [6, 23] and experimental studies [24, 25] have shown that as R increases the multiple cell convection will reverse to a unicellular convection through a step-by-step decrease in the number of cells. For high Pr fluids of present study, as shown in Figs. 2 and 7, the flow becomes increasingly chaotic as R increases for all the cases considered. The reverse transition to a unicellular flow has never been observed in the present experimental set up, in which all the laminar flows are observed to be two dimensional. This contradicts the tentative implication made by Le Quere [6] for low Pr fluid that the reverse transition to a unicellular convection is an intrinsic instability characteristic for the two dimensional flow.

To examine the possible existence of the hysteresis phenomenon for the present convective flow, we ran many tests increasing the ΔT first to a desirable value and then decreasing to the original ΔT. From the heat flux variation vs temperature difference (as shown in Fig. 9), no hysteresis was found. However, the hysteresis phenomenon can be detected from the wave number (a) variation vs R. As shown in Fig. 12 for the case of 80% solution, for instance, the backward route corresponding to decreasing ΔT deviates from the forward route to increasing ΔT. Note that the large uncertainty of the measurement of wavelength (and thus a) was due to the unsteady motion of convection, which resulted in an nonuniformity of the wavelength of convection cells. The hysteresis was observed for all the cases considered in the present study. The variation of a with R for all the cases considered are illustrated in Fig. 13, where the uncertainty is not shown. It is seen that the wave number in general decreases monotonically with increasing R (see also the flow patterns in Fig. 2), which is also true for low Pr case [6].

5. CONCLUDING REMARKS

From previous qualitative and quantitative descriptions, one may draw a clear picture about the natural convection in the vertical slot. For $R > R_1$, the primary flow gives up its stability to the unsteady secondary flow consisting of traveling vortices (or waves), in which the mergence of vortices prevails. The period of mergence is about 5 min on average. For $R > R_2$, the counter-rotating tertiary vortex occurs between secondary vortices. The tertiary vortex is not

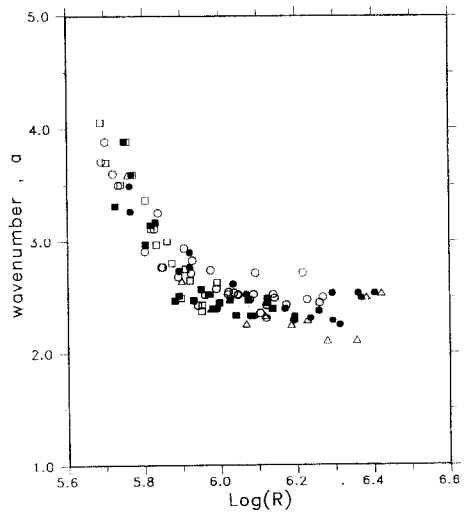

FIG. 13. The wave number vs Rayleigh number for all the cases considered in the present study. □: 90% solution; ■: 80% solution; ○: 70% solution; ●: 60% solution; △: 50% solution; ▲: 40% solution.

stable in the sense that it may either disappear and lead to a mergence of secondary vortices or degenerates into a secondary vortex and two new tertiary vortices after stretching of tertiary vortex occurs. With a tertiary vortex in between, the period of mergence of two secondary vortices can be up to about 10 min. For $R > R_3$, both the secondary and tertiary vortices within the slot are very unstable. A sequence of vortex merging-and-unmerging leads to a fully irregular turbulent flow. The multicellular convection, as R increases, never returns to the unicellular convection but becomes increasingly chaotic and eventually results in a turbulent flow. For all laminar flows observed in the present experiment, the heat transfer characteristics can be represented by the linear relationship of equation (3). This linear relation is independent of Pr and holds for both secondary and tertiary flows. The hysteresis phenomenon was observed for all the cases considered. The wavelength of the vortex in general increases with R. In conclusion, the varying viscosity as well as the large Pr of the working fluid are responsible for the occurrence of unsteady flows observed.

Recently, Kimoto and Miyawaki [26] and Kimoto [27] have reported that three dimensional secondary flow motions were found in their experiments. They conducted experiments in a box of 55 cm high × 11 cm deep × 5 cm wide, while filling the box with an 85% glycerin–water solution up to a height of 51 cm, thus, the aspect ratio of their experiment is approximately 10. By observing the fluid motion through the transparent hot wall, they found that the fluid in the core of the secondary vortex moves spirally towards the side wall facing the depth of the slot, then, as close to the side wall, moves spirally backwards along the periphery of the vortex; eventually, it vanished at the center of the slot. This spiral motion, nonetheless, was not found in the present experiment, which may be due to the following reasons. First, the aspect ratio of the slot, which as discussed in Gill and Kirkman [14] is crucial in determination of the flow characteristics in the vertical slot, is much smaller in Kimoto's box compared with ours. Secondly, they imposed a large temperature gradient ($R = 9 \times 10^5$) across the slot at the beginning of the experiment and fixed it to the end. This sudden imposing of a large temperature gradient may cause some sort of finite amplitude disturbances and leads the convective flow to a fully nonlinear regime in a short time. Consequently, one would expect to result in a completely different flow from that of the present experiment, in which a gradual increase of ΔT was imposed.

The precise mechanism driving the spiral vortex motion as found in Kimoto [27] is still unclear, which may merit a further study focusing on the effect due to Prandtl number, aspect ratio, or variable viscosity. The three dimensional flow, nevertheless, truly plays a crucial role in the stability characteristics of the flow in the vertical slot. To the authors' opinion, both the unsteadiness, as pointed out by the present study, and the three-dimensionality are worth paying attention to in the future.

Acknowledgement—The financial support for this work from the National Science Council through Grant No. NSC 82-0401-E-002-374 is greatly appreciated.

REFERENCES

1. J. W. Elder, Laminar free convection in a vertical slot, *J. Fluid Mech.* **23,** 77–98 (1965).
2. J. W. Elder, Turbulent free convection in a vertical slot, *J. Fluid Mech.* **23,** 99–111 (1965).
3. G. K. Batchelor, Heat transfer by free convection across a closed cavity between vertical boundaries at different temperature, *Q. Appl. Maths* **12,** 209–233 (1954).
4. A. E. Gill, The boundary-layer regime for convection in a rectangular cavity, *J. Fluid Mech.* **26,** 515–536 (1966).
5. Y. Lee and S. A. Korpela, Multicellular natural convection in a vertical slot, *J. Fluid Mech.* **126,** 91–121 (1983).
6. P. Le Quere, A note on multiple and unsteady solutions in two-dimensional convection in a tall cavity, *ASME Trans., J. Heat Transfer* **112,** 965–974 (1990).
7. P. Le Quere, Transition to unsteady natural convection in a tall water-filled cavity, *Phys. Fluids A* **2,** 503–515 (1990).
8. S. A. Korpela, D. Gozum and C. B. Baxi, On the stability of the conduction regime of natural convection in a vertical slot, *Int. J. Heat Mass Transfer* **16,** 1683–1690 (1973).
9. P. G. Daniels, Convection in a vertical slot, *J. Fluid Mech.* **176,** 419–441 (1987).
10. P. G. Daniels, Stationary instability of the convective flow between differentially heated vertical planes, *J. Fluid Mech.* **203,** 525–540 (1989).
11. P. G. Daniels and M. Weinstein, Nonlinear stability of convective flow between heated vertical planes, *J. Engng Math.* **23,** 377–386 (1989).
12. S. Tangam and C. F. Chen, Stability analysis on the convection of a variable viscosity fluid in an infinite vertical slot, *Phys. Fluids A* **29,** 1367–1372 (1986).
13. G. Lauriat and G. Desrayaud, Influences of the boundary conditions and linearization on the stability of a radiating fluid in a vertical layer, *Int. J. Heat Mass Transfer* **28,** 1613–1617 (1985).
14. A. E. Gill and C. C. Kirkham, A note on the stability of convection in a vertical slot, *J. Fluid Mech.* **42,** 125–127 (1970).
15. C. M. Vest and V. S. Arpaci, Stability of natural convection in a vertical slot, *J. Fluid Mech.* **36,** 1–15 (1969).
16. J. E. Hart, Stability of the flow in a differentially heated inclined slot, *J. Fluid Mech.* **47,** 547–576 (1971).
17. N. Seki, S. Fukusako and H. Inaba, Visual observation of natural convective flow in a narrow vertical cavity, *J. Fluid Mech.* **84,** 695–704 (1978).
18. C. F. Chen and S. Thangam, Convective stability of a variable-viscosity fluid in a vertical slot, *J. Fluid Mech.* **161,** 161–173 (1985).
19. P. G. Simpkins and J. E. Godreau, Onset of periodic convection in a vertical slot, *Phys. Fluids A* **1,** 1479–1483 (1989).
20. A. Chait and S. A. Korpela, The secondary flow and its stability for natural convection in a tall vertical enclosure, *J. Fluid Mech.* **200,** 189–216 (1989).
21. M. Nagata and F. H. Busse, Three-dimensional tertiary motions in a plane shear layer, *J. Fluid Mech.* **135,** 1–26 (1983).
22. Y.-M. Chen and A. J. Pearlstein, Stability of free-con-

vection flows of variable-viscosity fluids in vertical and inclined slots, *J. Fluid Mech.* **198,** 513–541 (1989).
23. B. Roux, J. Grondin, P. Bontoux and G. de Vahl Davis, Reverse transition from multicellular to monocellular motion in vertical fluid layer, *Phys. Chem. Hydro.* **3F,** 292–297 (1980).
24. J. F. Pignatel and J. F. Marcillat, Transition to time-dependent free convection in an inclined air layer, *Int. J. Heat Mass Transfer* **7,** 169–178 (1986).
25. A. Chikhaoui, J. F. Marcillat and R. L. Sani, Successive transitions in thermal convection within a vertical enclosure. In *Natural Convection in Enclosures, ASME HTD* 99, 29–35 (1988).
26. H. Kimoto and Y. Miyawaki, Three dimensional flow generated in the multicellular natural-convection field of a vertical slot, *Heat Transfer—Jap. Res.* **21**(1), 20–38 (1992).
27. H. Kimoto, On the three-dimensional flow generated in the natural convection fields of vertical rectangular slots *Proc. 2nd China–Japan Symp. of Visualization,* pp 402–409 (published by International Academic Publishers), Hangzhou, China (1992).